

TWO-ZONE DIFFUSION OF ELECTRONS AND POSITRONS FROM GEMINGA EXPLAINS THE POSITRON ANOMALY

KUN FANG,^{1,2} XIAO-JUN BI,^{1,2} PENG-FEI YIN,¹ AND QIANG YUAN^{3,4}

¹*Key Laboratory of Particle Astrophysics, Institute of High Energy Physics, Chinese Academy of Sciences, Beijing 100049, China*

²*School of Physics, University of Chinese Academy of Sciences, Beijing 100049, China*

³*Key Laboratory of Dark Matter and Space Astronomy, Purple Mountain Observatory, Chinese Academy of Sciences, Nanjing 210008, China*

⁴*School of Astronomy and Space Science, University of Science and Technology of China, Hefei, Anhui 230026, China*

(Dated: July 26, 2018)

ABSTRACT

The recent HAWC observations of very-high-energy γ -ray halo around Geminga and Monogem indicate a very slow diffusion of cosmic rays which results in tiny contribution of positrons from these two pulsars to the local flux. This makes the cosmic positron excess anomaly observed by PAMELA and AMS-02 even more puzzling. However, from the Boron-to-Carbon ratio data one can infer that the average diffusion coefficient in the Galaxy should be much larger. In this work we propose a two-zone diffusion model that the diffusion is slow only in a small region around the source, outside of which the propagation is as fast as usual. We find that such a scenario can naturally explain the positron excess data with parameters even more reasonable than that in the conventional one-zone diffusion model. The reason is that during the life time of Geminga (~ 300 kyr) the electrons/positrons have propagated too far away with a fast diffusion and lead to a low local flux. The slow diffusion region in the two-zone model helps to confine the electrons/positrons for a long time and lead to an enhancement of the local flux. So under the constraint of the HAWC observations, pulsars are still the probable origin of the cosmic-ray positron excess.

1. INTRODUCTION

The cosmic-ray positron excess has been discovered for nearly a decade (Adriani et al. 2009; Ackermann et al. 2012; Aguilar et al. 2013), but its origin is still a mystery. These extra positrons may originate either from astrophysical sources like pulsars or the dark matter annihilation/decay. Among various kinds of astrophysical sources, the Geminga pulsar (PSR J0633+1746) has been widely believed to be a very promising candidate to produce the positron excess (Yüksel et al. 2009; Hooper et al. 2009; Yin et al. 2013; Hooper et al. 2017). Geminga is one of the nearest pulsars with a distance of 250_{-62}^{+120} pc (Faherty et al. 2007). Its age is estimated to be about 3.42×10^5 years, and the derived spin-down energy is 1.23×10^{49} erg (Manchester et al. 2005; Fang et al. 2018). All these parameters suggest that Geminga can probably dominate the high energy positron flux observed on the Earth. The extended TeV γ -ray halo around Geminga pulsar observed by Milagro (Abdo et al. 2007) and HAWC (Abeysekara et al. 2017b) gives straightforward evidence supporting that Geminga can indeed generate very high energy electrons and positrons (e^\pm).

However, the detailed morphological study of the very high-energy γ -ray emission from Geminga and PSR B0656+14 (Monogem) by HAWC suggests that the e^\pm produced by these pulsars diffuse out significantly slower than that in the average interstellar medium (ISM) as inferred from the Boron-to-Carbon ratio (B/C) measurements (Abeysekara et al. 2017a). In such a case, the e^\pm produced by Geminga or Monogem can hardly reach the Earth, and thus these two pulsars may be unlikely to account for the positron excess. On the other hand, Hooper & Linden (2017) pointed out that this slow-diffusion scenario should not be representative even in the local environment. Since H.E.S.S. has detected high-energy e^\pm up to ~ 20 TeV¹, these e^\pm can only travel for $10 \sim 20$ pc within the cooling time given such a slow-diffusion condition. We can hardly find any high-energy e^\pm sources within such a small distance around the solar system.

Since the HAWC data can only probe a region of ~ 30 pc around Geminga and Monogem, it is very likely that the slow-diffusion region is actually limited in a small region around the sources, beyond which particles diffuse faster as typical Galactic cosmic rays. This scenario would be consistent with the B/C data and the H.E.S.S e^\pm spectrum (Hooper et al. 2017; Hooper & Linden 2017). In this work, we investigate whether this two-zone diffusion model can explain both the HAWC γ -ray data of Geminga and the positron excess. The two-zone diffusion model is solved with a

¹ <https://indico.snu.ac.kr/indico/event/15/session/5/contribution/694>

numerical method. Because the diffusion coefficient has a jump at the boundary between the two zones, the differencing scheme should be carefully dealt with.

In Section 2, we introduce the two-zone diffusion model and the numerical treatment to the propagation equation. In Section 3, we calculate the positron spectrum of Geminga in the two-zone scenario, and compare the result with the AMS-02 data (Aguilar et al. 2014). Then we conclude our work with some discussion in the last section.

2. METHOD

The propagation process of e^\pm can be described by the diffusion-cooling equation

$$\frac{\partial N}{\partial t} - \nabla(D\nabla N) - \frac{\partial}{\partial E}(bN) = Q, \quad (1)$$

where N is the differential number density of e^\pm , D denotes the diffusion coefficient, b is the energy-loss rate, and Q is the source term. In the present work, we are interested in the energy range higher than 10 GeV, so the convection and reacceleration terms which affect the low energy spectrum are neglected (Delahaye et al. 2009). The energy-loss rate has the form of $b(E) = b_0(E)E^2$, which describes the synchrotron and inverse Compton radiation cooling of e^\pm . The interstellar magnetic field in the Galaxy is set to be $3 \mu\text{G}$ to get the synchrotron term (Minter & Spangler 1996). For the inverse Compton scattering term, it is necessary to consider a relativistic correction to the scattering cross section. We follow the calculation of Schlickeiser & Ruppel (2010), where b_0 is energy-dependent.

The diffusion coefficient is usually assumed to be $D(E) = \beta^\eta D_0 (R/1 \text{ GV})^\delta$, where D_0 and δ are both constants, β is the velocity of particles in unit of light speed, η is a low energy correction parameter of the velocity dependence, and R is the rigidity. Assuming D is spatially constant, Yuan et al. (2017) constrained the propagation parameters with the B/C data of AMS-02 (Aguilar et al. 2016), and found that the best-fit model is the diffusion model with reacceleration. The obtained propagation parameters are $D_0 = (2.08 \pm 0.28) \times 10^{28} \text{ cm}^2 \text{ s}^{-1}$ and $\delta = 0.500 \pm 0.012$ (hereafter Y17 model). The thickness of the propagation halo is $z_h = 5.02 \pm 0.86 \text{ kpc}$, and the low energy correction parameter η is not relevant for this study.

For the e^\pm produced by Geminga, the propagation distance can be estimated as $2\sqrt{D(E)t_E}$, where $t_E = \min\{t_g, 1/(b_0 E)\}$, i.e., the smaller one of the age of Geminga t_g and the cooling time (Abeysekara et al. 2017a). If we adopt the propagation parameters of Y17, e^\pm of $\simeq 1 \text{ TeV}$ energies can diffuse to a distance of $\simeq 1.7 \text{ kpc}$. This scale is much smaller than z_h obtained in Y17. If the particles diffuse slower

in the region around Geminga, the total diffusion distance is even less. Therefore, it should be fine to assume a spherically symmetrical geometry of the propagation of e^\pm from Geminga. The diffusion coefficient for the two-zone model is then

$$D(E, r) = \begin{cases} D_1(E), & r < r_\star \\ D_2(E), & r \geq r_\star \end{cases}, \quad (2)$$

where r is the distance from Geminga, r_\star is the discontinuity shell of the diffusion coefficient, D_1 is the diffusion coefficient around Geminga which is inferred by the HAWC γ -ray data (Abeysekara et al. 2017a), and D_2 is the average diffusion coefficient in the Milky Way given by Y17. In a more realistic picture the diffusion coefficient may change gradually. However, no observations can constrain the transitional zone. Further as r_\star is a free parameter we can always get a equivalent result for the local e^\pm flux by adjusting r_\star in this simplified picture.

The spatially-dependent diffusion equation is difficult to be solved analytically, and we adopt a numerical method instead in this work. We assume that Geminga is a burst-like point source, then Equation (1) can be rewritten as following, along with the initial condition and the boundary conditions:

$$\begin{cases} \frac{\partial N}{\partial t} = \mathcal{L}N, \\ N(0, E, r) = Q(E)\delta(r), \\ N(t, E_{\max}, r) = 0, \\ \left. \frac{\partial N}{\partial r} \right|_{r=0} = 0, \\ N(t, E, r_{\max}) = 0, \end{cases} \quad (3)$$

where $E_{\max} = 500$ TeV, and $r_{\max} = 4$ kpc. The operator \mathcal{L} is the sum of the diffusion operator \mathcal{L}_r and the energy-loss operator \mathcal{L}_E , which are

$$\begin{aligned} \mathcal{L}_r &= \frac{1}{r^2} \frac{\partial}{\partial r} \left[r^2 D(r) \frac{\partial}{\partial r} \right], \\ \mathcal{L}_E &= b \frac{\partial}{\partial E} + \frac{\partial b}{\partial E}. \end{aligned} \quad (4)$$

We apply the *operator splitting method* to deal with the two operators separately. For the discretization of the energy-loss scheme, we follow the method given by Kissmann (2014), while for the diffusion operator, we use two different discretizations depending

on if r_i lies on the discontinuity surface (i is the spatial step index). If not, the well-known Crank-Nicolson scheme for constant D is a good choice. For the case of $r_i = r_*$, the difference equation should be re-written to ensure the conservation of the flux at both sides of the discontinuity surface. We adopt the *finite volume method* to derive the differencing scheme for this case. All the details of the discretization are presented in Appendix A. We should point out the differencing scheme derived by the *finite volume method* (Equation [A3]) is different from those used in GALPROP (Strong & Moskalenko 1998) or DRAGON (Evoli et al. 2008); the numerical schemes of GALPROP and DRAGON are basically applicable for continuously and slowly changed diffusion coefficient.

Then we describe the parameter settings. In the difference equation, the time step Δt is set to be 1000 years, which is much smaller than the age of Geminga. The spatial step Δr is 1 pc, then the initial condition given in Equation (A13) describes a spherical source with a radius of 1 pc. For an old source like Geminga, the spectrum at the Earth can be very close to that of a point source, especially when $E \gtrsim 100$ GeV (Thoudam & Hörandel 2012). We use a logarithmic scale with a ratio of 1.2 for the energy grids, that is, $E_{l+1}/E_l = 1.2$, where l is the energy step index. The e^\pm injection spectrum takes the form of $Q(E) = Q_0 E^{-\gamma}$, where $\gamma \simeq 2.2$, as indicated by the HAWC observation (Abeysekara et al. 2017a).

3. RESULT

If D is spatially uniform, Equation (1) can be solved analytically using the Green’s function method (Ginzburg & Syrovatskii 1964). We verify that our numerical solution for the one-zone case matches well with the analytical solution. For the two-zone diffusion case, there is no analytical way to test the results. To check that there is no “swallowing” or “spitting” of particles in the discontinuity surface, we integrate the number of particles, $N(r_i)$, for the two-zone diffusion cases with different r_* . We find that the number of particles is always the same as that of the one-zone cases. The present radial distributions of 1 TeV e^\pm are shown in Figure 1 for the two-zone diffusion scenarios and also the one-zone cases. Here we assume that all the spin-down energy of Geminga pulsar is converted to the energy of injected e^\pm (conversion efficiency), to determine the normalization.

The positron (or electron) spectra at the Earth generated by Geminga are shown in the left panel of Figure 2 for different r_* . The conversion efficiency of Geminga pulsar is also set to be 100%. The spectrum becomes harder for a larger r_* , since fewer low energy e^\pm can reach the Earth when the slow-diffusion zone is larger. The extreme cases of one-zone diffusion with Y17 or HAWC diffusion coefficients are also

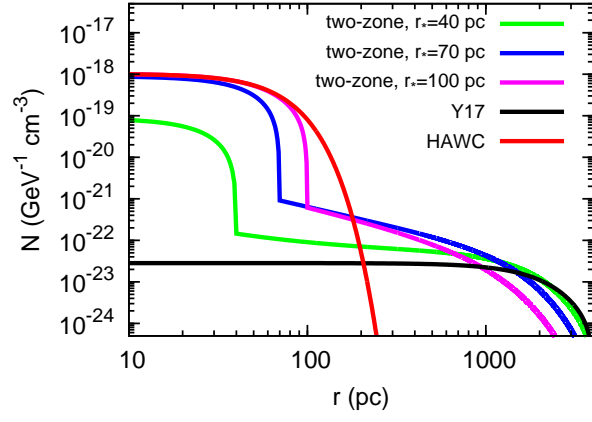


Figure 1. Radial distributions of 1 TeV e^\pm from Geminga at the present age. Three different r_* are adopted for the two-zone diffusion models. The distributions of the one-zone diffusion cases are also shown for comparison, the black line is for the one-zone diffusion model with Y17 diffusion coefficient, and the red line is calculated with parameters inferred by HAWC data [Abeysekara et al. \(2017a\)](#).

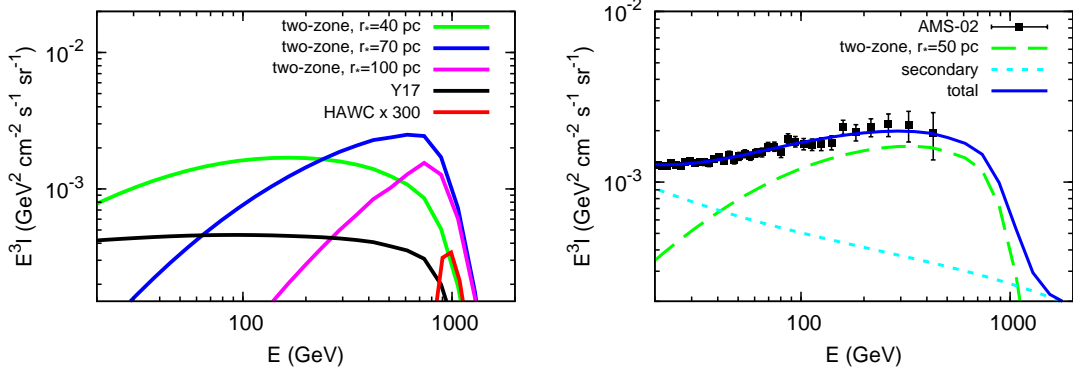


Figure 2. Left: expected electron (or positron) spectra of Geminga at the Earth. The conversion efficiency of Geminga pulsar is set to be 100%. Three different values of r_* are adopted for the two-zone diffusion scenario. The spectra of the one-zone diffusion cases with D_1 (HAWC) and D_2 (Y17) are also presented. Note the former is 300 times of its original spectrum. Right: the model predicted positron spectrum compared with the AMS-02 data ([Aguilar et al. 2014](#)). The green dashed line is the contribution of Geminga, with $r_* = 50$ pc and a conversion efficiency of 75%.

shown for comparison. We find that at high energies, the fluxes of the two-zone diffusion models are considerably higher than that of the one-zone diffusion case

with Y17 parameters. For a fast-diffusion model like Y17, the propagation scale of 1 TeV e^\pm of Geminga is $\simeq 1.7$ kpc. This scale is about 7 times larger than the distance between Geminga and the Earth, which implies that the particles have diffused to a considerably large region. For the two-zone diffusion scenario, the propagation of particles is hindered within the slow-diffusion zone. After being confined for some time in the inner region, these particles enter the fast propagation region and diffuse to the Earth. Since they spend less time in the fast-diffusion region, they can be effectively accumulated in a relatively smaller region and result in a higher flux at the Earth's location.

We find that the two-zone model with $r_\star = 50$ pc can well reproduce the AMS-02 data of the positron flux. The results for $r_\star > 50$ pc are too hard to explain the data, while the spectrum is too soft for the case with a smaller r_\star or the one-zone fast-diffusion model. Note that the final spectra depend on the injection spectrum of e^\pm assumed, which is $\gamma \simeq 2.2$ in this work. The comparison between the model and the data is shown in the right panel of Figure 2. Here the conversion efficiency to e^\pm is assumed to be 75% in order to match the data. For the secondary contribution from pp collisions, one can refer to Delahaye et al. (2009) and Fang et al. (2018).

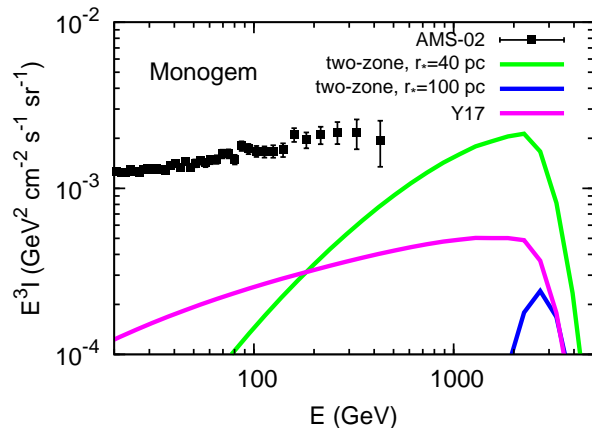


Figure 3. Positron spectra of Monogem with different diffusion models, compared with the AMS-02 data. The conversion efficiency is 100% for all the cases.

The e^\pm spectrum of Monogem under the two-zone diffusion can be obtained in the same way. The distance, age, and spin-down energy of Monogem is 290 pc, 1.1×10^5 years, and 1.58×10^{48} erg, respectively (Manchester et al. 2005). The observation of HAWC indicates a spectral index of ~ 2.0 for the injection spectrum of Monogem (Abeysekara et al. 2017a). As can be seen from Figure 3, the positron spectra of

Monogem is too hard to fit the AMS-02 data in the two-zone diffusion cases, due to its farther distance, younger age, and harder injection spectrum compared with Geminga. Thus Monogem cannot make a major contribution to the local positron fluxes even in the two-zone diffusion model.

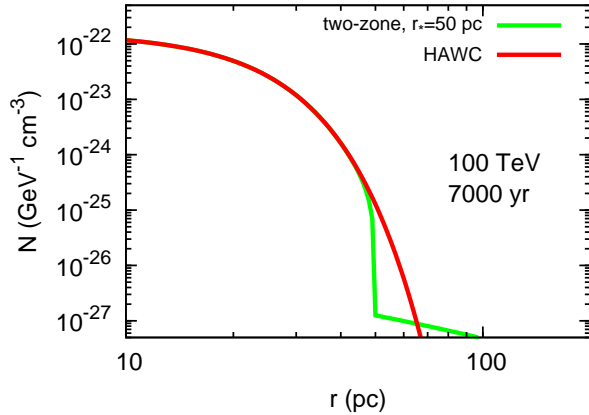


Figure 4. Density profiles of 100 TeV e^\pm with diffusion of 7000 years. The red line describes the slow-diffusion case proposed by [Abeysekara et al. \(2017a\)](#), while the green line represents the two-zone diffusion case with $r_\star = 50$ pc.

Finally we would like to give a simple self-consistency check if the two-zone region can reproduce the γ -ray profile observed by HAWC. The HAWC γ -ray data around 20 TeV are produced by ~ 100 TeV electrons, whose cooling time is about 7000 years. This indicates that the parent e^\pm of the γ -ray observed by HAWC should be younger than 7000 years. We show in Figure 4 the density profiles of 100 TeV e^\pm from Geminga with diffusion of 7000 years. Within 30 pc from Geminga, we find very good consistency between the one-zone slow-diffusion scenario of [Abeysekara et al. \(2017a\)](#) and the two-zone diffusion scenario with $r_\star = 50$ pc, which means the later proposed in this work can also accommodate the HAWC γ -ray data. The reason for this consistency is that 7000 years is too short for e^\pm to escape from the slow-diffusion region of the two-zone model.

4. CONCLUSION AND DISCUSSION

In this work we propose that a two-zone propagation scenario of cosmic ray e^\pm to account for the HAWC observations of extended halo around Geminga pulsar and the locally observed positron flux by AMS-02. The diffusion of e^\pm is assumed to be significantly slow within a distance of r_\star from the pulsar, as inferred by the spatial

brightness profile of γ -ray emission observed by HAWC (Abeysekara et al. 2017a). The particles diffuse beyond r_* with a diffusion coefficient inferred from the B/C data. A numerical method is adopted to solve the propagation equation, and the differencing scheme of the diffusion operator is derived by the *finite volume method*, which is different from those used in GALPROP or DRAGON.

The exact value of r_* to fit the AMS-02 positron flux degenerates with the injection spectrum of e^\pm , and hence can neither be too big nor too small. For larger (smaller) value of r_* , low energy particles would be confined in the slow-diffusion region longer (shorter), and the final positron spectrum is harder (softer). For an injection spectral index of ~ 2.2 and $r_* \sim 50$ pc, we find that the e^\pm from Geminga can reasonably account for the positron excess, with about 75% of the spin-down energy converted into e^\pm . Actually such a result is even more natural than that in the one-zone diffusion scenario which requires an efficiency even slightly larger than 100% (Yin et al. 2013).

The origin of the slow-diffusion zone around Geminga is still unclear. It is possible that the zone is pre-existed. For example, the shock of the parent supernova remnant (SNR) of Geminga, which is non-observable today, may have swept the ISM and made it more turbulent. Considering the age of 3×10^5 years, the shocked region can reach a size of ~ 100 pc (Yamazaki et al. 2006). We note that Geminga has a transverse velocity of 205_{-47}^{+90} km s $^{-1}$ (Faherty et al. 2007), which means a 70 pc offset from its birth place. So Geminga may still be within the shocked region of its SNR, where the diffusion coefficient is smaller. Meanwhile, if most of e^\pm are injected in the early age of Geminga, when the offset of Geminga is small and the scale of its SNR is not so large as today, our assumption of the symmetrical slow-diffusion zone may not be impacted.

Alternatively, the slow diffusion zone can be generated intrinsically by the e^\pm injected from Geminga. Near the cosmic-ray sources, the spatial gradient of particle density is significantly larger than that of the average ISM, which can lead to the growth of the streaming instability (Ptuskin et al. 2008; Malkov et al. 2013; D'Angelo et al. 2016). In this case, the magnetohydrodynamic turbulence may be considerably stronger than that in the ISM. Therefore, it is plausible that the e^\pm leaving Geminga are confined in the nearby zone for a longer time by the waves induced by themselves.

The slow-diffusion regions around pulsars may be common, which may result in extended γ -ray halos of pulsars and can probably explain the diffuse γ -ray excess observed in the Galactic plane (Abdo et al. 2008; Linden & Buckman 2017; Guo et al. 2016).

This work is supported by the National Key Program for Research and Development (No. 2016YFA0400200) and by the National Natural Science Foundation of China under Grants No. U1738209, 11475189, 11475191, 11722328. Q. Yuan acknowledges the 100 Talents Program of Chinese Academy of Science.

APPENDIX

A. DISCRETIZATION OF THE PROPAGATION EQUATION

We adopt the *operator splitting method* to divide the propagation equation into two one-dimensional sub-problems, and choose the *Strang splitting* which is second-order accurate (Strang 1968). We depict the flow chart as

$$N^n \xrightarrow[(t_n, t_{n+1/2})]{\mathcal{L}_E} \tilde{N}^{n+1/2} \xrightarrow[(t_n, t_{n+1})]{\mathcal{L}_r} N^{n+1/2} \xrightarrow[(t_{n+1/2}, t_{n+1})]{\mathcal{L}_E} N^{n+1},$$

where n is the time step index. Kissmann (2014) uses trapezoidal integration for the discretization of the energy-loss scheme, which leads to a second-order accuracy. The algebraic equation is written as

$$\begin{aligned} N_{l,i}^{n+1} = & \left(\frac{b_{l+1}\Delta t - \Delta E}{b_l\Delta t + \Delta E} \right) N_{l+1,i}^{n+1} - \left(\frac{b_l\Delta t - \Delta E}{b_l\Delta t + \Delta E} \right) N_{l,i}^n \\ & + \left(\frac{b_{l+1}\Delta t + \Delta E}{b_l\Delta t + \Delta E} \right) N_{l+1,i}^n, \end{aligned} \quad (\text{A1})$$

where l is the energy step index, i is the spatial step index, Δt denotes the time step, and $\Delta E = E_{l+1} - E_l$.

For the diffusion operator, we use two different discretizations, depending on if r_i lies on the discontinuity surface. If not, we apply the Crank-Nicolson scheme for constant D , which is second-order accurate and unconditionally stable. The corresponding algebraic equation is

$$\begin{aligned} & -\frac{D_{l,i}\Delta t}{2\Delta r^2} \left(1 - \frac{\Delta r}{r_i} \right) N_{l,i-1}^{n+1} + \left(1 + \frac{D_{l,i}\Delta t}{\Delta r^2} \right) N_{l,i}^{n+1} - \frac{D_{l,i}\Delta t}{2\Delta r^2} \left(1 + \frac{\Delta r}{r_i} \right) N_{l,i+1}^{n+1} \\ & = \frac{D_{l,i}\Delta t}{2\Delta r^2} \left(1 - \frac{\Delta r}{r_i} \right) N_{l,i-1}^n + \left(1 - \frac{D_{l,i}\Delta t}{\Delta r^2} \right) N_{l,i}^n + \frac{D_{l,i}\Delta t}{2\Delta r^2} \left(1 + \frac{\Delta r}{r_i} \right) N_{l,i+1}^n, \end{aligned} \quad (\text{A2})$$

where Δr is the radial step size, and $r_i = i\Delta r$. Equation (A2) is a tridiagonal system, which can be solved with LU decomposition. For the case of $r_i = r_*$, the difference equation should be re-written to ensure the conservation of the flux at

both sides of the discontinuity surface. We adopt the *finite volume method* to derive the differencing scheme for this case, which reads

$$\begin{aligned}
& -\frac{D_{l,i-1}\Delta t}{2\Delta r^2} \left(1 - \frac{\Delta r}{r_i}\right) N_{l,i-1}^{n+1} \\
& + \left[1 + \frac{D_{l,i-1}\Delta t}{2\Delta r^2} \left(1 - \frac{\Delta r}{r_i}\right) + \frac{D_{l,i+1}\Delta t}{2\Delta r^2} \left(1 + \frac{\Delta r}{r_i}\right)\right] N_{l,i}^{n+1} \\
& - \frac{D_{l,i+1}\Delta t}{2\Delta r^2} \left(1 + \frac{\Delta r}{r_i}\right) N_{l,i+1}^{n+1} \\
& = \frac{D_{l,i-1}\Delta t}{2\Delta r^2} \left(1 - \frac{\Delta r}{r_i}\right) N_{l,i-1}^n \\
& + \left[1 - \frac{D_{l,i-1}\Delta t}{2\Delta r^2} \left(1 - \frac{\Delta r}{r_i}\right) - \frac{D_{l,i+1}\Delta t}{2\Delta r^2} \left(1 + \frac{\Delta r}{r_i}\right)\right] N_{l,i}^n \\
& + \frac{D_{l,i+1}\Delta t}{2\Delta r^2} \left(1 + \frac{\Delta r}{r_i}\right) N_{l,i+1}^n .
\end{aligned} \tag{A3}$$

The derivation of this scheme is presented as follows.

Consider a diffusion equation

$$\frac{\partial N}{\partial t} - \frac{1}{r^2} \frac{\partial}{\partial r} \left[r^2 D(r) \frac{\partial N}{\partial r} \right] = 0, \tag{A4}$$

where $D(r)$ is defined in Equation (2). We set $F = r^2 D(r) \partial N / \partial r$, which is the particle flux in r . Then Equation (A4) can be rewritten as

$$\frac{\partial N r^2}{\partial t} = \frac{\partial F}{\partial r}. \tag{A5}$$

Assuming $r_i = r_*$, the continuity of particle density and flux should be satisfied:

$$\begin{cases} N(t, r_i - 0) = N(t, r_i + 0), \\ F(t, r_i - 0) = F(t, r_i + 0). \end{cases} \tag{A6}$$

We integrate Equation (A5) in the time range of $[t_n, t_{n+1}]$ and the radial range of $[r_{i-1/2}, r_{i+1/2}]$, where $r_{i\pm 1/2} = r_i \pm \Delta r/2$, and we obtain

$$\begin{aligned}
& \int_{r_{i-1/2}}^{r_{i+1/2}} [N(t_{n+1}, r) - N(t_n, r)] r^2 dr \\
&= \int_{t_n}^{t_{n+1}} \left[\int_{r_{i-1/2}}^{r_{i+1/2}} \frac{\partial}{\partial r} F(t, r) dr \right] dt \\
&= \int_{t_n}^{t_{n+1}} \left[\int_{r_{i-1/2}}^{r_i} \frac{\partial}{\partial r} F(t, r) dr + \int_{r_i}^{r_{i+1/2}} \frac{\partial}{\partial r} F(t, r) dr \right] dt \tag{A7} \\
&= \int_{t_n}^{t_{n+1}} \{ [F(t, r_i - 0) - F(t, r_{i-1/2})] + [F(t, r_{i+1/2}) - F(t, r_i + 0)] \} dt \\
&= \int_{t_n}^{t_{n+1}} [F(t, r_{i+1/2}) - F(t, r_{i-1/2})] dt.
\end{aligned}$$

On the other hand, we have $\partial N/\partial r = F/[r^2 D(r)]$ as defined above. Integrating this relation in $[r_i, r_{i+1}]$, we get

$$\begin{aligned}
N(t, r_{i+1}) - N(t, r_i) &= \int_{r_i}^{r_{i+1}} \frac{F(t, r)}{r^2 D(r)} dr \\
&\approx F(t, r_{i+1/2}) \int_{r_i}^{r_{i+1}} \frac{1}{r^2 D(r)} dr,
\end{aligned} \tag{A8}$$

which means

$$F(t, r_{i+1/2}) \approx \frac{N(t, r_{i+1}) - N(t, r_i)}{\int_{r_i}^{r_{i+1}} \frac{1}{r^2 D(r)} dr}. \tag{A9}$$

The expression of $F(t, r_{i-1/2})$ can be found similarly. The integral terms in Equation (A7) can be approximated by

$$\int_{r_{i-1/2}}^{r_{i+1/2}} N(t_n, r) r^2 dr \approx N(t_n, r_i) r_i^2 \Delta r \tag{A10}$$

and

$$\int_{t_n}^{t_{n+1}} F(t, r_{i+1/2}) dt \approx [F(t_{n+1}, r_{i+1/2}) + F(t_n, r_{i+1/2})] \Delta t / 2, \tag{A11}$$

where the latter corresponds to the Crank-Nicolson scheme. Combining Equation (A7) and (A9–A11), we finally obtain

$$\begin{aligned} \frac{N(t_{n+1}, r_i) - N(t_n, r_i)}{\Delta t} = & \\ \frac{D_{i+1} r_{i+1}}{2\Delta r^2 r_i} [N(t_{n+1}, r_{i+1}) - N(t_{n+1}, r_i) + N(t_n, r_{i+1}) - N(t_n, r_i)] & \quad (\text{A12}) \\ - \frac{D_{i-1} r_{i-1}}{2\Delta r^2 r_i} [N(t_{n+1}, r_i) - N(t_{n+1}, r_{i-1}) + N(t_n, r_i) - N(t_n, r_{i-1})], & \end{aligned}$$

which can be rewritten as Equation (A3).

Finally, the initial condition is approximated by a step function

$$N(0, E, r_i) = \begin{cases} Q'(E), & i \leq 1 \\ 0, & i > 1 \end{cases}, \quad (\text{A13})$$

where $Q'(E) = Q(E)/(4\pi r_1^3)$. For the inner spatial boundary condition, we handle it with $N(r_1) = N(r_{-1})$. Plugging this relation into Equation (A2), we can then obtain $N(r_0)$.

REFERENCES

- Abdo, A. A., Allen, B., Berley, D., et al. 2007, *ApJL*, 664, L91
- Abdo, A. A., Allen, B., Aune, T., et al. 2008, *ApJ*, 688, 1078
- Abeysekara, A. U., Albert, A., Alfaro, R., et al. 2017a, *Science*, 358, 911
- . 2017b, *ApJ*, 843, 40
- Ackermann, M., Ajello, M., Allafort, A., et al. 2012, *Physical Review Letters*, 108, 011103
- Adriani, O., Barbarino, G. C., Bazilevskaya, G. A., et al. 2009, *Nature*, 458, 607
- Aguilar, M., Alberti, G., Alpat, B., et al. 2013, *Physical Review Letters*, 110, 141102
- Aguilar, M., Aisa, D., Alvino, A., et al. 2014, *Physical Review Letters*, 113, 121102
- Aguilar, M., Ali Cavasonza, L., Ambrosi, G., et al. 2016, *Physical Review Letters*, 117, 231102
- D' Angelo, M., Blasi, P., & Amato, E. 2016, *PhRvD*, 94, 083003
- Delahaye, T., Lineros, R., Donato, F., et al. 2009, *A&A*, 501, 821
- Evoli, C., Gaggero, D., Grasso, D., & Maccione, L. 2008, *JCAP*, 10, 018
- Faherty, J., Walter, F. M., & Anderson, J. 2007, *Ap&SS*, 308, 225
- Fang, K., Bi, X.-J., & Yin, P.-F. 2018, *ApJ*, 854, 57
- Ginzburg, V. L., & Syrovatskii, S. I. 1964, *The Origin of Cosmic Rays*

- Guo, Y.-Q., Hu, H.-B., & Tian, Z. 2016, Chinese Physics C, 40, 115001
- Hooper, D., Blasi, P., & Dario Serpico, P. 2009, JCAP, 1, 25
- Hooper, D., Cholis, I., Linden, T., & Fang, K. 2017, PhRvD, 96, 103013
- Hooper, D., & Linden, T. 2017, ArXiv e-prints, arXiv:1711.07482
- Kissmann, R. 2014, Astroparticle Physics, 55, 37
- Linden, T., & Buckman, B. J. 2017, ArXiv e-prints, arXiv:1707.01905
- Malkov, M. A., Diamond, P. H., Sagdeev, R. Z., et al. 2013, ApJ, 768, 73
- Manchester, R. N., Hobbs, G. B., Teoh, A., & Hobbs, M. 2005, AJ, 129, 1993
- Minter, A. H., & Spangler, S. R. 1996, ApJ, 458, 194
- Ptuskin, V. S., Zirakashvili, V. N., & Plesser, A. A. 2008, Advances in Space Research, 42, 486
- Schlickeiser, R., & Ruppel, J. 2010, New Journal of Physics, 12, 033044
- Strang, G. 1968, SIAM Journal on Numerical Analysis, 5, 506
- Strong, A. W., & Moskalenko, I. V. 1998, ApJ, 509, 212
- Thoudam, S., & Hörandel, J. R. 2012, MNRAS, 419, 624
- Yamazaki, R., Kohri, K., Bamba, A., et al. 2006, MNRAS, 371, 1975
- Yin, P.-F., Yu, Z.-H., Yuan, Q., & Bi, X.-J. 2013, PhRvD, 88, 023001
- Yuan, Q., Lin, S.-J., Fang, K., & Bi, X.-J. 2017, PhRvD, 95, 083007
- Yüksel, H., Kistler, M. D., & Stanev, T. 2009, Physical Review Letters, 103, 051101